Can a Coarse-grained Water Model Capture the Key Physical Features of the Hydrophobic Effect?

Kuntal Ghosh, Timothy D. Loose, and Gregory A. Voth*

Department of Chemistry, Chicago Center for Theoretical Chemistry, James Franck Institute, and Institute for Biophysical Dynamics, The University of Chicago, Chicago, IL 60637, USA

*Corresponding Author: gavoth@uchicago.edu

ABSTRACT

Coarse-grained (CG) Molecular Dynamics can be a powerful method for probing complex processes. However, most CG force fields use pairwise non-bonded interaction potentials sets, which can limit their ability to capture complex multi-body phenomena such as the hydrophobic effect. As the hydrophobic effect primarily manifests itself due to the non-polar solute affecting the nearby hydrogen bonding network in water, capturing such effects using a simple one CG site or "bead" water model is a challenge. In this work, we systematically test the ability of CG one site water models for capturing critical features of the solvent environment around a hydrophobe as well as the Potential of Mean Force (PMF) of neopentane association. We study two bottom-up water models: a Simple Pairwise (SP) Force-Matched water model constructed using the Multiscale Coarse-

Graining method and the Bottom-Up Many-Body Projected Water (BUMPer) model, which has three-body correlations implicitly embedded into it. We also test the top-down monatomic (mW) and the Machine Learned mW (ML-mW) water models. We find that the top-down models perform well in capturing the structural correlation in the water functions near the hydrophobe, but not the energetics of the PMF. BUMPer outperforms the SP water model in capturing structural correlations, but also gives an accurate PMF in contrast to the two mW models. Our study highlights the importance of including three-body interactions in CG water models, either explicitly or implicitly, while in general highlighting the applicability of bottom-up CG water models for studying hydrophobic association effects in a quantitative fashion.

I. INTRODUCTION

In recent years, Coarse-Grained Molecular Dynamics (CG-MD) simulations have garnered a lot of attention for its ability to computationally model complex chemical, biomolecular and condensed matter phenomena.[1-4] CG-MD effectively reduces the dimensionality of the system by integrating out fast degrees of freedom, leading to a simplified energy landscape, thus permitting larger timesteps in MD simulations. However, owing to the loss of information, capturing atomistic properties through CG-MD or simply CG simulations is a challenge. Broadly speaking, there are two approaches for constructing CG models, top-down and bottom-up.[1, 3, 4] Top-down CG models[5] are constructed directly from observable macroscopic and/or thermodynamic experimental data. However, they lack a rigorous statistical mechanical foundation and top-down models such as the MARTINI model[6] suffer from accuracy issues arising from an incorrect enthalpy-entropy decomposition of free energies.[7] Bottom-up CG methods ,[1] such as the Multiscale Coarse-Graining (MS-CG)[8-11] method, Iterative Boltzmann inversion (IBI),[12] Reverse Monte Carlo (RMC)[13] and Relative Entropy Minimization (REM)[14, 15] are constructed from a statistical mechanical framework. Recently, there has also been significant interest in using Machine Learning (ML) techniques to develop CG-MD

2

models.[16-25] The MS-CG and REM methods in particular are capable of determining the many-body potential of mean force (PMF, i.e., the free energy surface) for the statistical distribution of the CG sites or "beads" in the system that corresponds to the exact distribution from the all-atom system projected by CG mappings onto the CG sites. However, the challenge in all such approaches is how to express the many-body PMF either mathematically or numerically because that PMF is generally not known. As a result, approximation are often made such as assuming the non-bonded CG interactions are pairwise decomposable. In that vein, it is these sometimes neglected multi-body interactions that can lead to additional or stronger multi-body correlations which in turn may render a CG model based on a simpler expression of the CG PMF less accurate than desired.[26] In this paper, we explore one of the most fundamental of multi-body effects in the liquid state or in other soft matter systems, i.e., the hydrophobic effect.

Hydrophobic effects are fundamental to many processes such as protein folding and self-assembly.[27-31] Physically, the hydrophobic effects arise in water when the hydrogen bonded network of the liquid is affected by the presence of a non-polar solute, usually resulting in a multi-molecule structuring (correlation) of the water solvent hydrogen-bond network and hence a lowering of the system entropy, which in turn causes the free energy to increase (this is the primary reason for the insoluble nature of smaller hydrophobes in water). In turn, the system may aggregate the hydrophobes in an attempt to minimize the increase in free energy.

The dependence of hydrophobic effects on the solute size,[32-37] solute-solvent attractions,[37, 38] ionic strength,[39] temperature[33] and pressure[40] has also been the subject of numerous studies. When a small solute is immersed in water, as noted in the last paragraph, the water molecules in the immediate vicinity of the solute can rearrange amongst themselves to maintain the hydrogen bonds, albeit at the aforementioned entropic cost. Increasing the size of the solute beyond a certain cutoff causes the disruption of these hydrogen bonds: an entropic as well as an enthalpic effect. Historically, this effect has captured much interest and several experimental studies[41-46] and theoretical treatments[34, 35, 37, 47-50] were put forward to explain the essence of

3

hydrophobicity. The Lum-Chandler-Weeks[34] theory, in particular, gives a mathematical treatment of hydrophobicity at both short and long length scales as well as the crossover between them. However, such hydrophobic effects are particularly difficult to capture owing to their inherent multi-body nature[51]. Scaled particle theory and its modifications[52] provide an explicit mathematical treatment of such multi-body effects.

Hydrophobicity essentially has two aspects – hydration and association. Hydrophobic hydration at room temperature is typically characterised by a negative entropy of solvation and a large positive heat capacity.[35, 53, 54] Hydrophobic association, or the association of two non-polar solutes in water, has very interesting thermodynamic consequences. In particular, the PMF of hydrophobic association[32, 55] reveals very distinct features: a contact minimum (CM), a desolvation barrier (DB) and a solvent-separated minimum (SSM). All these effects have been studied extensively using All-Atom (AA) molecular dynamics (MD) models,[32, 40, 55] but to the best of our knowledge, such effects have never been studied using a CG model, including bottom-up ones. It is important to emphasize that both entropy and enthalpy play significant roles here,[35, 53, 56, 57] thus a rigorous bottom-up CG model would appear to be necessary.

Although MS-CG has proven itself to be a robust and powerful approach for carrying out CG simulations, as noted earlier it typically uses pairwise basis sets for representing the CG force fields.[10, 11, 58, 59] Previous studies have shown that such pairwise basis sets are somewhat lacking in reproducing the AA structural correlation functions in bulk water,[26, 60] where strong hydrogen bonding determines the local tetrahedral network.[61-64] As the hydrophobic effect primarily manifests itself due to the modified hydrogen bonded network in water in the presence of a hydrophobe, capturing such effects using any CG model with pairwise basis sets is indeed a challenge. It becomes even more complicated due to a lack of an explicit description of hydrogen bonding in a one CG bead water model (as the hydrogen atoms are not explicitly represented).

One natural way to overcome the limitation of having no explicit hydrogen bonds in a one CG bead water model is to explicitly incorporate three-body interactions in the CG force field.[26, 65, 66] It has been shown previously that CG water models employing three-

4

body interactions, such as the "top-down" monatomic or mW model,[66] and the bottom-up three-body MS-CG model,[26] can recapitulate structural properties of pure bulk water remarkably well. The recently developed Machine Learned mW model (ML-mW)[17] has been shown to improve upon the original mW model across several metrics, including the description of the liquid water density anomaly. Recently, Jin et al developed the Bottom-Up Many-Body Projected Water (BUMPer)[60, 67] model. BUMPer, which has three-body correlations projected onto pairwise basis sets, was shown to improve upon Simple Pairwise (SP) CG water in predicting structural correlations and anomalous properties of bulk water.

The main goal of this work is therefore to test the accuracy of a subset of both top-down and bottom-up CG water models in capturing the hydrophobic effect[32, 55] for a simple hydrophobe, neopentane, in water. It is also of clear interest to establish to the extent possible the physical accuracy of these CG models in that regard. As the PMF of neopentane association in water has been well studied using AA MD,[32, 55] and since neopentane has been suggested to be a small solute demonstrating a few of the properties of macroscopic hydrophobic objects,[32] it presents an excellent system for testing the CG models.

The remainder of this article is organized as follows: In Section II, all the theory and methods used, namely the MS-CG methodology and ways to incorporate three-body correlations such as in BUMPer, are discussed in detail. The computational details, including the details and constructions of the CG models used are also discussed there. We then present the results and analysis in Section III. It must be mentioned that throughout the article, the terms All-Atom (AA) and Fine-Grained (FG) have been used interchangeably. Similarly, neopentane has also been referred to as simply the hydrophobe several times throughout the text.

II. THEORY AND METHODS

A. The Multiscale Coarse-Graining (MS-CG) approach

In the MS-CG framework, FG systems are mapped to CG models, under the constraint of thermodynamic consistency and they also have a close connection to aspects of liquid state theory:[68]

$$p_{\mathrm{CG}}(\mathbf{R}^N, \mathbf{P}^N) \ = \ \int d\mathbf{r}^n \delta(\mathbf{M}(\mathbf{r}^n) \ - \ \mathbf{R}^N) \int d\mathbf{p}^n \delta(\mathbf{M}(\mathbf{p}^n) \ - \ \mathbf{P}^N) \, p_{\mathrm{FG}}(\mathbf{r}^n, \mathbf{p}^n)$$

Eq (1)

$$U_{CG}(\mathbf{R}^N) \ = \ -k_B T \ln \int d\mathbf{r}^n \delta(\mathbf{M}(\mathbf{r}^n) \ - \ \mathbf{R}^N) \exp\left(-\frac{u_{FG}(\mathbf{r}^n)}{k_B T}\right) \ + \ (const.)$$

Eq (2)

In Eq (1) and Eq (2), p_{FG} and p_{CG} refer to the probability distributions of the FG and CG systems. Similarly, u_{FG} refers to potential energy of the FG system, whereas U_{CG} refers to the many-body PMF of the CG system. The CG variables or beads are generated from the FG variables using a mapping operator[10, 11] ($\mathbf{M}_{\mathrm{I}}(\mathbf{r}) = \sum_i c_{Ii} \mathbf{r}_i$). Thereafter, a variational calculation is performed sometimes called Force-Matching (FM),[8-11, 59] which aims at minimizing the force residual (χ^2) between the projected FG forces (**f**) at their corresponding CG site, and the CG forces (**F**) (Eq (3)), such that

$$\chi^2 \ = \ \frac{1}{3N} \langle \sum_{I=1}^{N} \left| \mathbf{F}_I(\mathrm{M}(\mathbf{r}^n)) - \mathbf{f}_I(\mathbf{r}^n) \right|^2 \rangle$$

Eq (3)

However, typically the CG potentials (the negative gradient of which yields **F**) are expanded in terms of a "basis set" of numerical functions such as B-spline functions existing of pairwise (or two-body) interactions only for simple one CG bead systems such as a liquid.[59] But, the simple pairwise interaction approximation is generally unable to capture the multi-body correlations of water,[26, 60] where strong anisotropic effects are important.[63, 64] Even though it has been shown that MS-CG implicitly accounts to a certain

6

degree for three-body correlations through the Yvon-Born-Green equation,[68] it is still limited by the use of pairwise basis sets. Several modifications of MS-CG have been proposed over the years, including Ultra Coarse-Graining (UCG)[69-71] and CG with virtual sites (VCG);[25, 72-74] however, a direct way to account for such effects is to account for three-body or higher interactions (e.g., in the MS-CG scheme).

B. Projecting three-body correlations onto pairwise basis sets: Bottom-Up Many-Body Projected Water (BUMPer)

One natural step in the development of CG models is the incorporation of three-body effects [26]. In addition to pairwise basis sets, functions explicitly incorporating three-body interactions can be added to the overall basis set (Eq (4)). Subsequent FM yields a CG potential with three-body interactions.

$$U_{3b} = \sum_{I} \sum_{J>I} U_{3b}^{(2)}(R_{IJ}) + \sum_{I} \sum_{J \neq I} \sum_{K>J} U_{3b}^{(3)}(\theta_{JIK}, R_{IJ}, R_{IK})$$

Eq (4)

Here, the notation $U_{3b}^{(2)}(R_{IJ})$ refers to the two-body interaction in a potential that includes three-body terms, hence the subscript "3b". In general, $U_{3b}^{(2)}$ can, e.g., be expressed as a linear combination of spline functions as basis sets. However, instead of using spline functions for the three-body term, Larini et al.[26] used the Stillinger-Weber (SW) function as the basis set:

$$U^{(3)}(\theta_{JIK}, R_{IJ}, R_{IK}) =$$
$$\lambda_{JIK} \varepsilon_{JIK} (cos\theta_{JIK} - \cos\theta_0)^2 \exp\left(\frac{\gamma_{IJ}\sigma_{IJ}}{R_{IJ} - a_{IJ}\sigma_{IJ}}\right) \exp\left(\frac{\gamma_{IK}\sigma_{IK}}{R_{IK} - a_{IK}\sigma_{IK}}\right) \quad \text{Eq (5)}$$

where, λ and ε refer to the interaction strength and units, γ is a parameter to tune the decay of the potential, a is the non-bonded cutoff, θ_0 is the equilibrium triplet angle and

7

σ is the length unit. Explicit incorporation of these three-body interaction has then been shown to greatly improve the reproduction of structural properties of the CG water system. However, this model is still limited by its computational cost. Thus, it was desirable to develop a CG model which can successfully strike a balance between accuracy and computational cost, while retaining the effects of higher-body interactions. This led to the development of the Bottom-Up Many-Body Projected Water (BUMPer) model.[60, 67] BUMPer aims to project the three-body interactions onto effective pairwise basis sets. After an AA simulation followed by CG mapping, for a given triplet *JIK* with the central CG bead labelled as *I*, a three-body conditional probability $p(\theta_{JIK}, R_{IK} | R_{IJ})$, is introduced which finds the probability at which R_{IK} and θ_{JIK} take some specific values for a given R_{IJ}. This conditional probability satisfies the relation:

$$\int d\theta_{JIK} dR_{IK} p(\theta_{JIK}, R_{IK} | R_{IJ}) = 1 \qquad \text{Eq (6)}$$

An ensemble average is carried out over the conditional probability to get the effective interactions as a function of only one distance.

$$\begin{aligned} U_{eff}^{(2)}(R_{IJ}) &= \langle U^{(3)}(\theta_{JIK}, R_{IJ}, R_{IK}) \rangle_{p(\theta_{JIK}, R_{IK}|R_{IJ})} \\ &= 2(N_c - 1) \int d\theta_{JIK} dR_{IK} p(\theta_{JIK}, R_{IK} | R_{IJ}) U^{(3)}(\theta_{JIK}, R_{IJ}, R_{IK}) \end{aligned}$$

$$\text{Eq (7)}$$

where, $2(N_c - 1)$ is a pre-factor accounting for the counting of the forces (N_c being the coordination number).

Henceforth, the overall CG effective potential can be written as,

$$\begin{aligned} U(\mathbf{R}^N) = \sum_I \sum_{J>I} \Big\{ &U_{3b}^{(2)}(R_{IJ}) \\ &+ 2(N_c - 1) \int d\theta_{JIK} dR_{IK} p(\theta_{JIK}, R_{IK} | R_{IJ}) U_{3b}^{(3)}(\theta_{JIK}, R_{IJ}, R_{IK}) \Big\} \end{aligned}$$

$$\text{Eq (8)}$$

It is important to note that for this model, the three-body interactions are imposed only up to 3.7 Å (also the cutoff for computing N_c), which roughly corresponds to the first solvation shell of water, where short-range effects dominate the local hydrogen bonding

8

network. Thus, to correct for the long-range interactions, Iterative Force-Matching (IFM)[75] is carried out. The resulting effective pair potential is the BUMPer model.

i. Merits of BUMPer

A comparative analysis of a CG mapped AA model, SP, and BUMPer water reveals that unlike SP potentials, BUMPer is capable of accurately reproducing both two-body and three-body structural correlation functions in water.[60, 67] Moreover, temperature transferable BUMPer models were constructed using a free energy decomposition scheme[76] and the model was shown to capture the growth of ice at the ice/water interface.[67] Statistical mechanical calculations also suggest that BUMPer can capture certain anomalies of water.[67] Thus, it is important to see if BUMPer can capture the hydrophobic effect, as this effect involves multi-body correlations and should be especially challenging for a one bead CG water model.

C. The mW and the ML-mW water models

The monatomic water (mW) model[66] is a top-down one CG bead water model which also employs the three-body Stillinger-Weber interaction. Specifically, the two-body and three-body interactions are given by –

$$U_{\mathrm{mW}}\left(\theta_{JIK}, R_{IJ}, R_{IK}\right)$$

$$= \sum_{J>I} \left\{ A\varepsilon \left[B\left(\frac{\sigma}{R_{IJ}}\right)^4 - 1\right] \exp\left(\frac{\sigma}{R_{IJ} - a\sigma}\right)\right\}$$

$$+ \sum_{J\neq I} \sum_{K>J} \left\{ \lambda\varepsilon[\cos\theta_{JIK} - \cos\theta_0]^2 \times \exp\left(\frac{\gamma\sigma}{R_{IJ} - a\sigma}\right)\exp\left(\frac{\gamma\sigma}{R_{IK} - a\sigma}\right)\right\}$$

$$\text{Eq (9)}$$

where $A = 7.049556277$, $B = 0.6022245584$, $\theta_0 = 109.47$°, $\varepsilon = 6.189$ kcal/mol, $\sigma = 2.3925$Å, $a = 1.8$, $\lambda = 23.15$, and $\gamma = 1.2$. In the original mW paper the model was shown to capture the tetrahedral network of liquid water along with other properties including energetics, phase transitions and density, heat capacity and diffusion anomalies, albeit for some of

those properties one must remain keenly aware of the "representability" problem[77] as the calculated properties may not have a direct correspondence with the underlying FG ones. Even though the mW model has been previously used for investigating the PMF of methane-methane association in a top-down fashion[78], it remains to be seen if it can used for neopentane, which is a significantly larger hydrophobe than methane (in the context of the length scale dependence of the hydrophobic effect[34]).

The ML-mW model is a re-parameterized version of the original mW model, using a multi-level hierarchical optimization machine learning strategy. The advantages of ML-mW over mW, as well as the parameters used in the ML-mW model can be found in Ref.[17]

D. Computational details

i. AA setup of the neopentane in water system

For computing the distribution functions, a system of one neopentane immersed in a water box of 900 water molecules was set up. The box dimensions taken were $30.2 \times 30.2 \times 30.2$ Å^3 under periodic boundary conditions (PBC). Water was modelled using the SPC/Fw[79] model, while OPLS-AA[80] interactions were used for neopentane. All cross interactions were computed using the standard Lorentz-Berthelot mixing rules.[81] A 12 Å cutoff was used for the long-range non-bonded interactions, coupled with a particle-particle particle-mesh solver[82, 83] with a precision of 10^{-4}. For all AA simulations, the timestep was set as 2 fs. The structures were constructed and visualized using Packmol,[84] Avogadro[85] and VMD,[86] and all simulations were carried out with the Large-scale Atomic/Molecular Massively Parallel Simulator (LAMMPS)[87] package. After minimization using the conjugate gradient method and a short constant NPT equilibration (2 ns), a production constant NVT run with the Nosé-Hoover thermostat was carried out for 20 ns, with frames being printed after every 1 ps, for subsequent construction of the CG models. For computing the PMF of hydrophobe association, two hydrophobes were taken in the water box of said dimensions.

10

ii. CG setup and construction of pair potentials

The AA systems were first mapped to CG beads using a center of mass (COM) mapping operator, with both neopentane and water represented as single CG beads. The pair potentials were then generated by FM using the MSCGFM package[59] and the recently released OpenMSCG package.[88] For two-body FM, the CG force field was expressed as a linear combination of sixth-order B-splines, with a resolution of 0.1 Å and 15 Å as the outer cutoff. Inner cut-offs for the water-hydrophobe and hydrophobe-hydrophobe interactions were taken as 3.36 Å and 4.99 Å respectively. Details about the AA simulations of bulk water, two-body FM and three-body FM for constructing water-water pair potentials can be found in the Supplementary Material and in Ref.[26, 60] The SW parameters in Eq (5) were chosen as follows: a_{IJ} = 3.7 Å (at the COM resolution), γ_{IJ} = 1.2, ε_{JIK} = 1 kcal/mol and σ_{IJ} = 1 Å. Following Eq (6) and Eq (7), three-body correlations were projected onto pairwise basis sets (Eq (8)), and finally IFM was carried out to obtain BUMPer. The box dimensions were kept the same as the AA simulations, and the timestep used for all CG simulations was 5 fs. BUMPer is performant at timesteps of 8 or even 10 fs[26, 60], but this is not the focus of the current work. The constant NVT production runs were carried out for 20 ns, with frames being printed after every 1 ps. The temperature for both the AA and CG simulations was set at 300 K. It is important to emphasize that the water-water interactions used throughout our CG runs were parameterized separately from bulk water simulations (as in Ref.[26, 60]), to test the transferability of the CG water models.

iii. The CG models

For computing the radial and angular distribution functions, a system of one hydrophobe immersed in water was simulated, the purpose being to check the behaviour of the water-hydrophobe pairs and triplets. For computing the PMF of hydrophobe association, two hydrophobes were simulated in the solvent. In both cases, the CG mapped AA model (denoted simply as AA) and six CG models were taken - the Simple Pairwise model (denoted as SP), the BUMPer model (denoted as BUMPer) and two variations each of the mW and ML-mW models. Simple pairwise FM potentials were used for the water-

11

hydrophobe interactions in the SP and BUMPer models. The water-water interactions were modelled using the simple pairwise FM and BUMPer pair potentials in the SP and BUMPer models. Two separate cases were chosen for the mW models as it is a top-down model so the choice is not automatic. These two choices of the water-hydrophobe interaction were (1) modelled as simple pairwise force-matched (the model thereby being denoted as mW-FM), and (2) a second using Boltzmann inversion (BI) ($U_{nw} = -k_B T \ln g_{nw}(r)$) of the AA water-hydrophobe RDF (hence called the mW-BI model). Similarly, FM and BI variants were constructed for the ML-mW models (denoted as ML-mW-FM and ML-mW-BI). For all the CG models, the hydrophobe-hydrophobe potential was constructed using simple pairwise FM. It should be noted that instead of a system of one hydrophobe in water, a system of twenty hydrophobes immersed in 980 water molecules was taken for constructing the hydrophobe-hydrophobe CG potentials, to ensure sufficient sampling of the said interactions.

iv. Computing the PMF of neopentane association

Umbrella Sampling[89] was used for sampling the configuration space in a system of two neopentane molecules immersed in bulk water. Harmonic biasing potentials were imposed on the distance (ξ) between the centre of masses of the two hydrophobes.

$$V(\xi) = k(\xi - d_0)^2$$

Eq (10)

The force constant (k) was taken to be 2 kcal/mol/Å^2 for all the AA and CG simulations.[32, 55] The simulations comprised 20 windows (each carried out for 40 ns) such that the equilibrium distance (d_0) for each window ranged from 3.5, 4.0, ..., to 13.0 Å. The resulting distribution profiles were combined using the Weighted Histogram Analysis Method (WHAM)[90-92] to generate the free energy profile for hydrophobe association. To compute the final PMF, the Jacobian of the coordinate transformation was also accounted for by adding $2k_B T \ln \xi$ to the free energy obtained from WHAM. It was also ensured that the PMF decays to zero at large distances by adding an offset. All these simulations were carried out using the PLUMED[93, 94] plugin in the LAMMPS package.

12

III. RESULTS AND DISCUSSION

A. *Pair potentials*

Figure 1 shows the pair potentials used for all the CG models: Fig. 1a shows the water-water pair potentials constructed from MSCGFM using simple pairwise basis sets, and the BUMPer potential (constructed separately from bulk water simulations). Figure 1b shows the two variants of the water-hydrophobe pair potential – the FM variant used in the SP, BUMPer, mW-FM and ML-mW-FM models and the BI pair potential used in the mW-BI and ML-mW-BI models. Finally, Fig. 1c shows the hydrophobe-hydrophobe FM potential used for all the CG models.
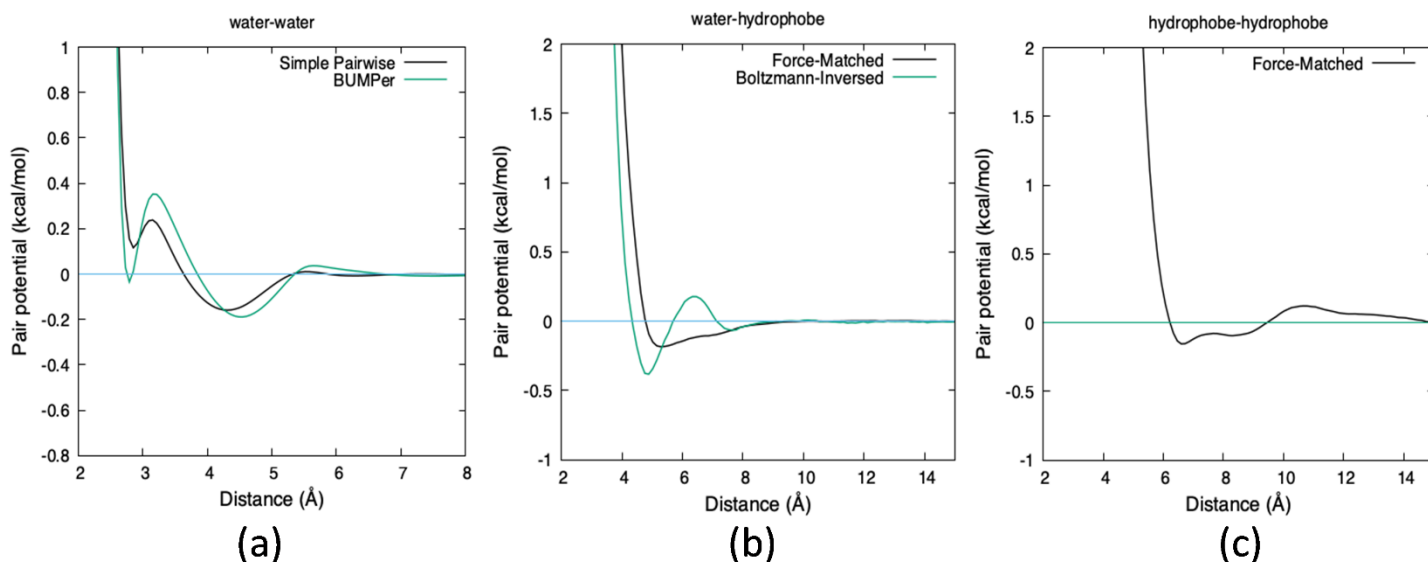

Figure 1 : (a) SP and BUMPer pair potentials for water-water interactions (b) FM and BI pair potentials for the water-hydrophobe interactions (c) FM pair potential for the hydrophobe-hydrophobe interactions

B. *Radial distribution functions*

The radial distribution function (RDF) lies at the heart of the statistical mechanics of fluids,[61, 62] and hence is an important metric to assess the accuracy and validity of our CG models. The RDF is given by,

13

$$g(R) = \frac{V}{N^2} \langle \sum_I \sum_{J \neq I} \delta(R - R_{IJ}) \rangle$$

<div align="right">Eq (11)</div>

where V is the volume of the simulation box, and I and J denote particle indices (FG or CG). The RDF obtained from a CG simulation reflects the ability of that CG model to capture pairwise structural correlations. In the context of the hydrophobic effect, the goal of a CG model is to accurately recapitulate the AA RDF of the solvent-solvent and solvent-hydrophobe pairs. To this end, we computed the RDFs from the CG simulations corresponding to each CG model taken. We note that we only consider the water molecules/beads within the first two solvation shells of the hydrophobe (~ 9.5 Å) for the water-water RDF. Owing to the superior performance of the FM variants over the BI ones, only the RDFs using mW-FM and ML-mW-FM are presented in the main text. The reader is directed to the Supplementary Information (SI) for the complete set of results using all the models.
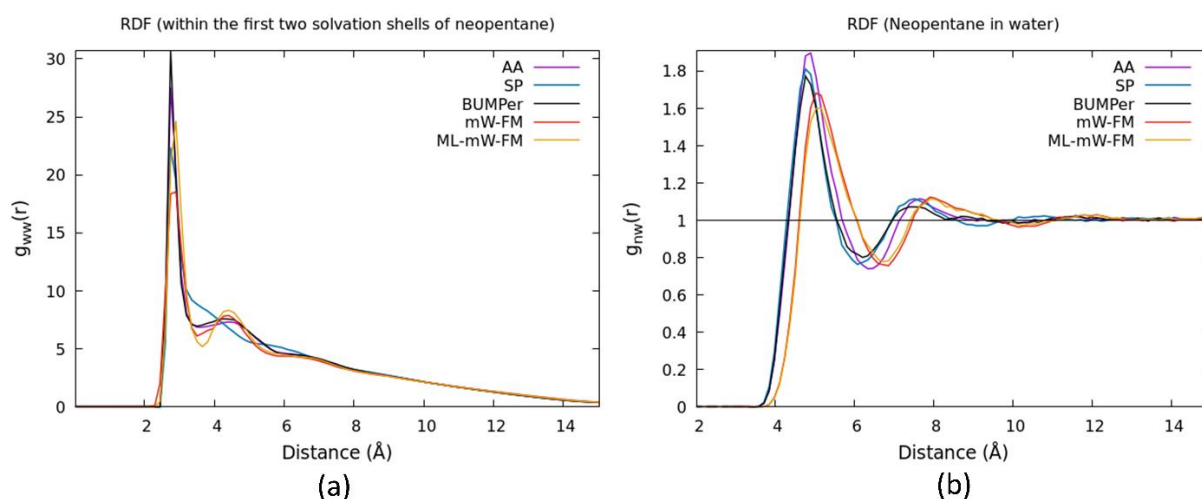

Figure 2 : (a) Water-water RDF considering only the water molecules in the first two solvation shells of neopentane (b) Neopentane-water RDF. See text for discussion of these results.

<div align="center">14</div>

Table 1: Coordination numbers - For the water-water pairs (water molecules within first two solvation shells of neopentane considered only)

Cut-off (Å)	AA	SP	BUMPer	mW-FM	mW-BI	ML-mW-FM	ML-mW-BI
3.7	4.2	4.3	4.1	4.0	4.1	4.0	4.1
4.5	7.3	7.4	7.2	7.3	7.5	7.1	7.3
5.7	13.3	13.0	13.1	13.0	13.6	12.7	13.5

Table 2: Deviation (in percentage) in the coordination numbers from the AA data for the water-water pairs (water molecules within first two solvation shells of neopentane considered only)

Cutoff (Å)	SP	BUMPer	mW-FM	mW-BI	ML-mW-FM	ML-mW-BI
3.7	2.7	2.1	3.7	2.0	4.4	2.5
4.5	1.9	1.0	0.041	2.7	2.6	0.62
5.7	2.5	1.6	2.4	2.4	4.3	1.1

Figure 2 (and Figure S1 of the SI) depicts the RDFs of the hydrophobe in water, and the water-water pairs across all the models taken. It is clear from the figures that the bottom-up models (SP and BUMPer) do remarkably well in capturing the AA hydrophobe in water RDF, with minor deviations at the first peak. However, the first solvation shell is shifted for both. The mW-FM and ML-mW-FM models are also slightly shifted, with the first minimum shifted by ~ 5% from the AA one. Both the BI models yield a much more structured RDF (Figure S1), with significant deviations in both the peaks and the minima. The solvent-solvent RDF is well replicated by BUMPer and the mW and ML-mW models. It is also important to note that ML-mW-FM (9 % deviation in g(r) at the first peak) shows significant improvement over mW-FM (30% deviation) in capturing the first solvation

15

shell in the water-water RDF and is almost as good as BUMPer (9%). However, unsurprisingly, SP is unable to capture this, as has been documented before.[26, 60]

To quantify the accuracy of the models, coordination numbers (CN) about the central atom were also calculated. The coordination number is given by,

$$N_c = 4\pi\rho_\beta \int_0^{R_c} g_{\alpha\beta}(R)R^2\ dR$$

<div align="right">Eq (12)</div>

where, β is the central atom about which the number of α atoms (FG or CG) are counted. ρ_β is the density of β particles and R_c refers to the cutoff up to which the CN is computed.

For the water-water pairs (Tables 1 and 2), three cut-offs were chosen for computing the CNs - 3.7 Å, 4.5 Å and 5.7 Å, which roughly corresponds to the first solvation shell, the second correlation peak, and the second solvation shell. While mW-FM has the lowest deviation from AA for the 4.5 Å cut-off, and mW-BI for the 3.7 Å cutoff, it can be seen that overall BUMPer does well. Furthermore, Tables 3 and 4 reveal that within the first solvation shell of neopentane (6.5 Å), both the mW models do very well and for the second solvation shell, SP, BUMPer, and mW-FM are comparable. It is also interesting to note that the CN of water becomes around 30 within the first solvation shell of the hydrophobe (as opposed to ∼ 6 in bulk water up to the 3.7 Å cut-off [60]).

Table 3: Coordination numbers - For the neopentane-water pairs

Cut-off (Å)	AA	SP	BUMPer	mW-FM	mW-BI	ML-mW-FM	ML-mW-BI
6.5	32.7	31.5	31.5	32.0	32.1	31.3	31.8
9.5	113.5	112.5	112.9	112.6	115.1	112.2	114.8

Table 4: Deviation (in percentage) in the coordination numbers from the AA data for the neopentane-water pairs

Cut-off (Å)	SP	BUMPer	mW-FM	mW-BI	ML-mW-FM	ML-mW-BI
6.5	3.7	3.5	2.1	1.8	4.2	2.8
9.5	0.82	0.53	0.74	1.4	1.2	1.2

C. Angular distribution functions

The angular distribution function (ADF) is given by,

$$P(\theta) = \frac{1}{W}\langle\sum_I \sum_{J \neq I} \sum_{K > J} \delta(\theta - \theta_{IJK})\rangle$$

Eq (13)

where W is a normalization factor depending on the bin width and the number of frames of the trajectory, and indices I, J and K refer to the particles. Like the RDF, to test how well a CG model can capture three-body correlations, it is important to carry out a comparative analysis between the AA and CG ADFs. In this work, we computed the ADFs of the various triplets at a distance from the simulation of a single hydrophobe in water, again considering only the water CG beads within the first two solvation shells of the hydrophobe for the water-water-water ADFs. Here again, we present only the results using the FM variants, the remainder can be found in the SI. Moreover, only a detailed look into the significant correlation peaks of the ADFs are presented here for simplicity; the reader is directed to the SI for the complete ADFs from all the models.
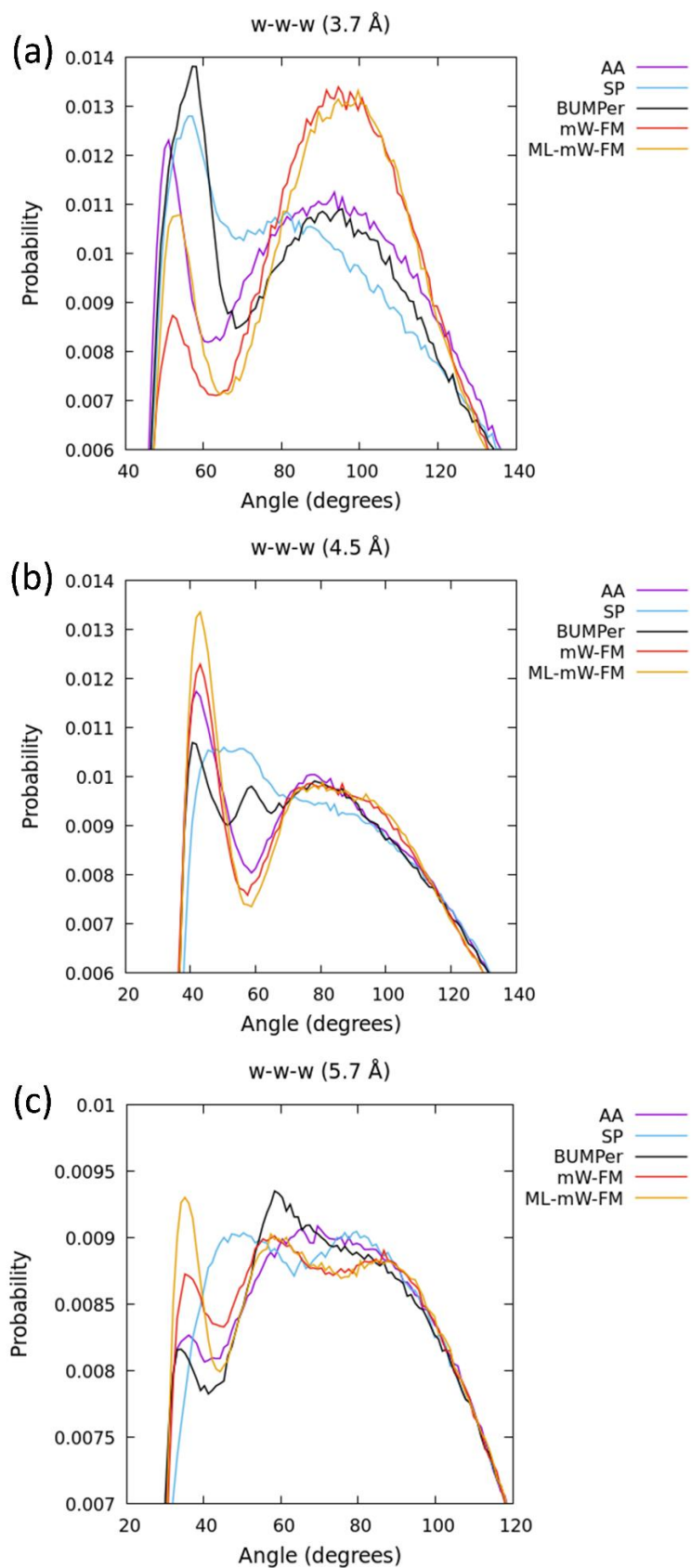
17

Figure 3 : Water-water-water ADFs (a) within first solvation shell of water (b) up to the second correlation peak (c) within the second solvation shell of water. See text for discussion of these results.
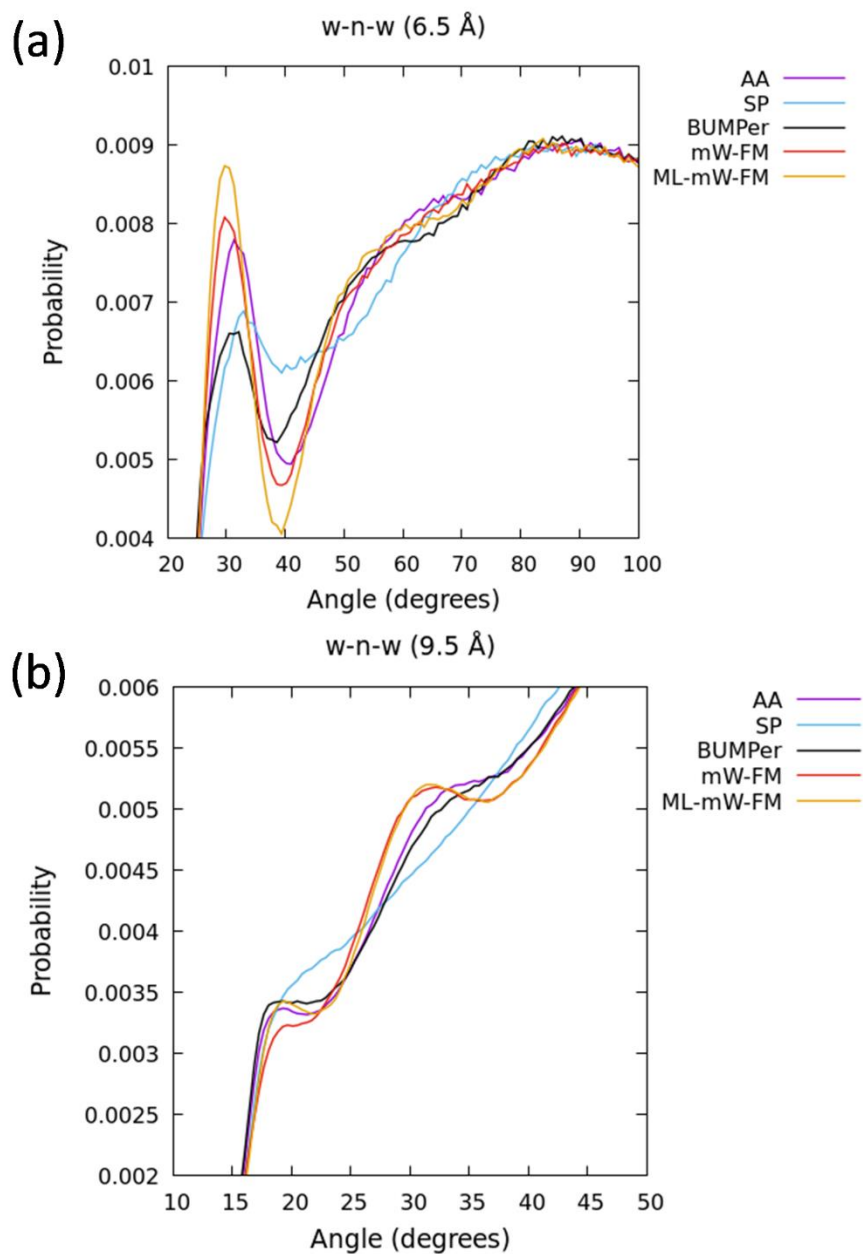
18

Figure 4 : Water-neopentane-water ADFs (a) within first solvation shell of neopentane (b) within the first two solvation shells of neopentane. See text for discussion of these results.
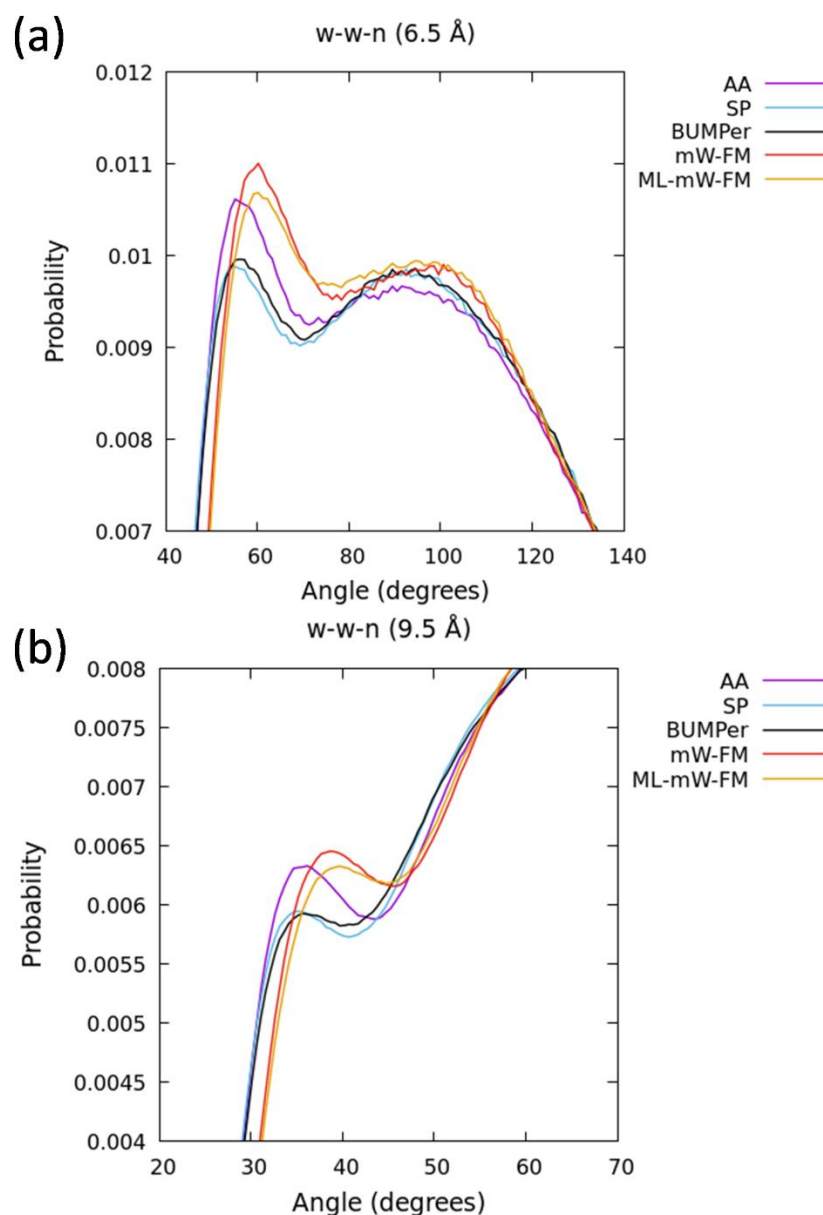
Figure 5 : Water-water-neopentane ADFs (a) within first solvation shell of neopentane (b) within the first two solvation shells of neopentane. See text for discussion of these results.

Figure 3 (and Figure S2) shows the ADFs of the water-water-water triplets for three different cutoffs (similar to the RDF analysis) - 3.7 Å, 4.5 Å and 5.7 Å. While SP cannot accurately capture the two local maxima in the AA ADF (for 3.7 Å) at $\sim 50°$ and $\sim 100°$, BUMPer can, even though the first peak is shifted to $\sim 60°$. Interestingly, in the short range, both the mW models lead to an interchange between their two maxima. As the mW water model is specifically designed to capture the tetrahedral structure of water, mW-

20

FM does well in capturing the AA ADF at 4.5 Å. Moreover, up to the 4.5 Å and 5.7 Å cutoffs, mW-FM outperforms ML-mW-FM, but within the short-range 3.7 Å cut-off, ML-mW-FM shows closer correspondence to the first correlation peak in the exact AA CG projected water-water-water ADFs than mW-FM. In general, ML-mW generates higher first correlation peaks than mW for the water-water-water triplets. The SP model fails significantly, while BUMPer does somewhat better, but not as well as the mW models. As the cutoff is further increased to 5.7 Å, it is again evident that SP does not do as well as the other CG models.

It is also of importance to inspect the ADFs for the heterogeneous triplets: water-neopentane-water (Figures 4 and S3) and water-water-neopentane (Figures 5 and S4) triplets. Both the mW models (particularly mW-FM) give water-neopentane-water ADFs close to their atomistic counterparts in this case. While BUMPer slightly underestimates the intensity of the first correlation peak by about 15% and the minimum by about 6% with a slight shift of about 3.7%, SP can capture neither the first peak (12% error) nor the minimum (24% error), within the 6.5 Å cutoff.

A significant conclusion cannot be drawn from the water-water-neopentane ADFs, except for the fact that both mW-BI and ML-mW-BI are unable to reproduce these ADFs. Both of these models show significant over-structuring of the triplet, while BUMPer exhibits an under structuring.

21

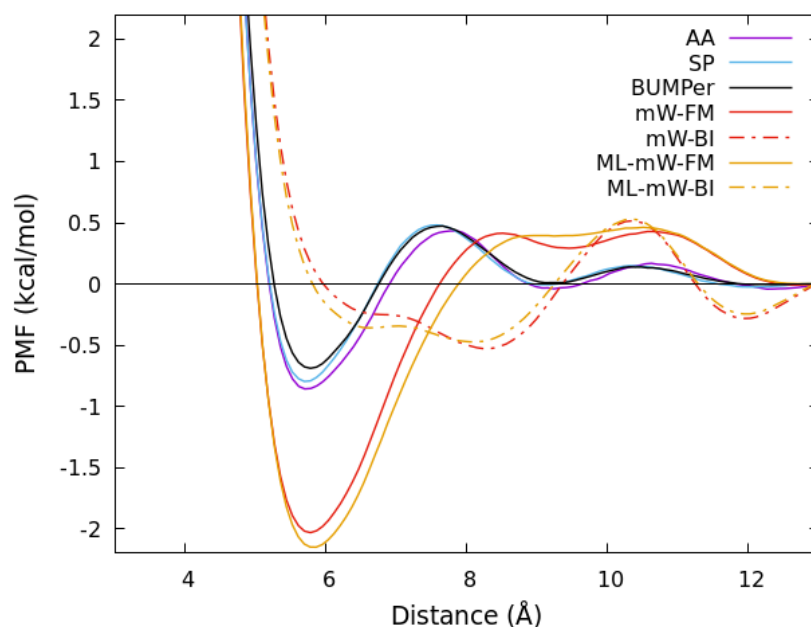## D. Potential of Mean Force of CG neopentane association in CG water

Figure 6 : The PMF of neopentane association in water using different CG models in comparison to the AA model (the error is of the order of 10^{-2} kcal/mol)

The PMF of hydrophobic association in water is perhaps the most stringent and important test of the ability of a CG water model to capture the hydrophobic effect. As can be seen from Figure 6, the bottom-up approaches, SP and BUMPer, are able to capture the key features of the free energy profile remarkably well, i.e., the global minimum (~ 5.8 Å), the desolvation barrier (~ 7.7 Å) and the solvent separated minimum (~ 9.2 Å). Interestingly, despite not having three-body interactions explicitly embedded into it, SP can accurately capture the key features of the PMF. This corroborates well with Ref. [68] which suggests that the MS-CG method, by its inherent statistical mechanical framework, should be able to capture to some degree both two-body and three-body correlations. Even though pairwise basis sets limit its ability to accurately capture the RDFs and ADFs (Figures 2 and 3), it is still able to capture energetics of dissolving two solutes in a polar solvent. Even though there is no explicit description of hydrogen bonding in our CG systems, the fact that both SP and BUMPer can capture the essential features of the PMF suggests that they are indirectly able to capture the effects of the disruption of the hydrogen bonded network in water due to the hydrophobes. Such a distorted hydrogen

bonded network has been documented previously through both AA simulations[32, 55] and spectroscopic studies.[46]

On the other hand, the mW and ML-mW models fail to capture such features of the PMF. The mW-FM and ML-mW-FM potentials can correctly predict the neopentane-neopentane distance corresponding to the contact minimum, but the depth of the minimum is off by more than a factor of two for both mW-FM and ML-mW-FM, and they are unable to capture the correct solvent separated minimum as well as the desolvation barrier. Instead, they have a shifted desolvation barrier with a very shallow solvent separated minimum at 9.4 Å. Both mW-BI and ML-mW-BI, on the other hand, fail to capture any of the three critical features of the CG projected AA PMF. The reader is referred to the SI for details of the error analysis of the PMF.

It is also important to emphasize the transferability of some of the CG water models, especially the BUMPer model. Both the SP and BUMPer models were parameterized separately from bulk water simulations. Three-body interactions were imposed only on the water-water-water triplets; thus BUMPer could capture the PMF without any need to parameterize the heterogeneous water-neopentane triplets. The mW and ML-mW models by contrast are not transferable, at least in terms of calculating the PMF of hydrophobic association.

IV.   CONCLUSIONS

Capturing multi-body effects such as the hydrophobic effect using CG models is a challenge, even systematically constructed ones. This is inherently due in part to the limitations in the basis sets chosen for constructing the CG models, which are usually pairwise (or two-body) in nature. In particular, capturing the complex interactions between the hydrogen bonds of water and a non-polar solute using coarse-graining is very difficult. In this work, we explore this issue by constructing CG models to probe the Potential of Mean Force of hydrophobe (in our case, neopentane) association in water. We constructed six CG models - SP, BUMPer, mW-FM, mW-BI, ML-mW-FM and ML-mW-

23

BI. The first two models are bottom-up models employing Simple Pairwise and BUMPer pair potentials for water-water interactions, and the rest are CG models using the top-down monatomic water (mW) and ML-mW potentials.

We studied the corresponding radial and angular distribution functions of the neopentane in water system using our six CG models. Our tests show that BUMPer, the mW, and ML-mW models can accurately capture the water-water RDFs, while SP fails to do so due to its pairwise basis sets. For the hydrophobe in water RDF, except mW-BI and ML-mW-BI, the CG models do reasonably well in capturing the AA RDF. Interestingly, while the mW models are very good at replicating the AA homogeneous solvent triplet ADFs beyond the first solvation shell, they give inversely ordered peaks in the short-range region. Furthermore, mW models do give accurate water-hydrophobe-water ADFs when compared to their AA counterparts projected on to the CG sites. While SP does not do well in capturing these distribution functions, BUMPer does much better, though not as good as the mW models for this particular ADF.

In terms of the PMF for hydrophobe association – which is the most important property studied in this work – the bottom-up models significantly outperform the top-down mW and ML-mW models. Both the SP and BUMPer models can accurately capture the most significant features of the PMF of neopentane association in water, despite the very coarse-grained one bead model used for neopentane, and despite SP not having multi-body correlations explicitly embedded into it. In contrast, the mW and ML-mW models fail to capture any of the important features of the PMF. This highlights the capacity of bottom-up CG methods, when properly formulated such as BUMPer, for studying multi-body effects such as the hydrophobic effect.

As was noted before, the SP and BUMPer water models were separately parameterized from bulk water simulations alone. Thus, despite not explicitly accounting for the hydrophobe(s) in the simulations used for constructing these water-water CG potentials, they were still able to capture the hydrophobic effect. The models, and

especially BUMPer, thus exhibit a clear degree of transferability for having a hydrophobe (or at least two) added to them.

Overall, it can also be concluded that the mW and ML-mW models are reasonably well suited for studying distribution functions in the hydrophobe-water systems, but not for capturing the PMF of hydrophobe association. Recently, it has also been found that mW differs from TIP4P in capturing the kinetics of nucleation and growth of methane clathrate hydrates.[95]

As far as BUMPer is concerned, not only was it able to yield accurate RDFs and reasonably good ADFs across all the cutoffs taken, it was also able to yield an accurate PMF of neopentane association. This leads us to conclude that BUMPer is indeed a very powerful, bottom-up one bead CG water model, which can be used for more complex systems. One natural way to improve upon the BUMPer method in the future is to explicitly incorporate heterogeneous or hybrid three-body interactions (up to reasonable and physically meaningful cutoffs), and project them onto pairwise basis sets. Though the development of a generalized BUMPer method is not the goal of the current work, the existing methodology can be extended to hybrid triplets (depending on the system being studied) and will be the subject of a future work. Furthermore, as is already well-known in literature, CG models offer substantial speed-up compared to the AA models,[1, 3, 60] and thus this work could successfully point to the merit of using bottom-up CG models such as BUMPer for capturing complex multi-body phenomena. Although attempts have been made recently to incorporate multi-body effects in CG force fields using neural networks, [20] such CG neural network potentials based MD simulations are significantly slower than simulations using more conventional pairwise CG potentials. Our work therefore opens a new direction to be pursued in the future: the development and application of systematically constructed bottom-up CG models for studying hydrophobic effects in complex systems such as proteins and membranes.

SUPPLEMENTARY MATERIAL

See the Supplementary Information for (i) Details on the AA simulations of bulk water and constructing Simple Pairwise and BUMPer pair potentials from them (ii) Complete radial and angular distribution profiles for all the models used (iii) A representative example of proof of convergence of the PMF with error bars and the plots of the probability distribution for each simulation window

ACKNOWLEDGMENTS

DATA AVAILABILITY

The data that support the findings of this study are available from the corresponding author upon request.

REFERENCES

1.   J. Jin, A. J. Pak, A. E. P. Durumeric, T. D. Loose and G. A. Voth, J. Chem. Theory Comput. **18**, 5759 (2022).
2.   M. G. Saunders and G. A. Voth, Annu. Rev. Biophys. **42**, 73 (2013).
3.   W. G. Noid, J. Chem. Phys. **139**, 090901 (2013).
4.   S. Dhamankar and M. A. Webb, J. Poly. Sci. **59**, 2613 (2021).
5.   P. C. T. Souza, R. Alessandri, J. Barnoud, S. Thallmair, I. Faustino, F. Grunewald, I. Patmanidis, H. Abdizadeh, B. M. H. Bruininks, T. A. Wassenaar, P. C. Kroon, J. Melcr, V. Nieto, V. Corradi, H. M. Khan, J. Domanski, M. Javanainen, H. Martinez-Seara, N. Reuter, R. B. Best, I. Vattulainen, L. Monticelli, X. Periole, D. P. Tieleman, A. H. de Vries and S. J. Marrink, Nat. Methods. **18**, 382 (2021).

6.   S. J. Marrink, H. J. Risselada, S. Yefimov, D. P. Tieleman and A. H. de Vries, J. Phys. Chem. B **111**, 7812 (2007).

7.   Z. Jarin, J. Newhouse and G. A. Voth, J. Chem. Theory Comp. **17**, 1170 (2021).

8.   S. Izvekov and G. A. Voth, J. Phys. Chem. B **109**, 2469 (2005).

9.   S. Izvekov and G. A. Voth, J. Chem. Phys. **123**, 134105 (2005).

10.   W. G. Noid, J. W. Chu, G. S. Ayton, V. Krishna, S. Izvekov, G. A. Voth, A. Das and H. C. Andersen, J. Chem. Phys. **128**, 244114 (2008).

11.   W. G. Noid, P. Liu, Y. Wang, J. W. Chu, G. S. Ayton, S. Izvekov, H. C. Andersen and G. A. Voth, J. Chem. Phys. **128**, 244115 (2008).

12.   D. Reith, M. Putz and F. Muller-Plathe, J. Comp. Chem. **24**, 1624 (2003).

13.   A. P. Lyubartsev and A. Laaksonen, Phys. Rev. E **52**, 3730 (1995).

14.   M. S. Shell, J. Chem. Phys. **129**, 144108 (2008).

15.   A. Chaimovich and M. S. Shell, J. Chem. Phys. **134**, 094112 (2011).

16.   J. Wang, S. Olsson, C. Wehmeyer, A. Perez, N. E. Charron, G. de Fabritiis, F. Noe and C. Clementi, ACS Cent. Sci. **5**, 755 (2019).

17.   H. Chan, M. J. Cherukara, B. Narayanan, T. D. Loeffler, C. Benmore, S. K. Gray and S. K. R. S. Sankaranarayanan, Nat. Commun. **10** (2019).

18.   P. Gkeka, G. Stoltz, A. B. Farimani, Z. Belkacemi, M. Ceriotti, J. D. Chodera, A. R. Dinner, A. L. Ferguson, J. B. Maillet, H. Minoux, C. Peter, F. Pietrucci, A. Silveira, A. Tkatchenko, Z. Trstanova, R. Wiewiora and T. Lelievre, J. Chem. Theory Comput. **16**, 4757 (2020).

19.   A. E. P. Durumeric and G. A. Voth, J. Chem. Phys. **151**, 124110 (2019).

20.   J. Wang, N. Charron, B. Husic, S. Olsson, F. Noe and C. Clementi, J. Chem. Phys. **154**, 164113 (2021).

21.   D. Dhabal, S. Sankaranarayanan and V. Molinero, J. Phys. Chem. B **126**, 9881 (2022).

22.   D. Dhabal and V. Molinero, J. Phys. Chem. B **127**, 2847 (2023).

23.   F. G. Mattioli, F. Sciortino and J. Russo, J. Chem. Phys. **158**, 104501 (2023).

24.   A. E. P. Durumeric, N. E. Charron, C. Templeton, F. Musil, K. Bonneau, A. S. Pasos-Trejo, Y. Chen, A. Kelkar, F. Noe and C. Clementi, Curr. Opin. Struct. Biol. **79**, 102533 (2023).

25.   P. G. Sahrmann, T. D. Loose, A. E. P. Durumeric and G. A. Voth, J. Chem. Theory Comput. **19**, 4402 (2023).

26.   L. Larini, L. Lu and G. A. Voth, J. Chem. Phys. **132**, 164107 (2010).

27.   B. Kronberg, M. Costas and R. Silveston, J. Disper. Sci. Technol. **15**, 333 (1994).

28.   B. Kronberg, Curr. Opin. Colloid In. **22**, 14 (2016).

29.   D. Chandler, Nature **437**, 640 (2005).

30.   D. March, V. Bianco and G. Franzese, Polymers-Basel **13**, 156 (2021).

31.   D. Ben-Amotz, J. Phys. Chem. Lett. **6**, 1696 (2015).

32.   X. Huang, C. J. Margulis and B. J. Berne, J. Phys. Chem. B **107**, 11742 (2003).

33.   R. Zangi and B. J. Berne, J. Phys. Chem. B **112**, 8634 (2008).

34.   K. Lum, D. Chandler and J. D. Weeks, J. Phys. Chem. B **103**, 4570 (1999).

35.   N. Choudhury and B. M. Pettitt, J. Phys. Chem. B **110**, 8459 (2006).

36.   G. Graziano, J. Chem. Soc. Faraday T **94**, 3345 (1998).

37.   N. Choudhury and B. M. Pettitt, J. Am. Chem. Soc. **127**, 3556 (2005).

38.   D. M. Huang and D. Chandler, J. Phys. Chem. B **106**, 2047 (2002).

39.   M. Bogunia and M. Makowski, J. Phys. Chem. B **124**, 10326 (2020).

40.   R. Sarma and S. Paul, J. Chem. Phys. **136**, 114510 (2012).

41.   M. Rigby and J. M. Prausnitz, J. Phys. Chem. **72**, 330 (1968).

27

42. A. H. Narten and H. A. Levy, J. Chem. Phys. **55**, 2263 (1971).
43. I. M. Abdulagatov, A. R. Bazaev and A. E. Ramazanova, J. Chem. Thermodyn. **25**, 249 (1993).
44. B. M. Rankin, D. Ben-Amotz, S. T. van der Post and H. J. Bakker, J. Phys. Chem. Lett. **6**, 688 (2015).
45. A. A. Bakulin, M. S. Pshenichnikov, H. J. Bakker and C. Petersen, J. Phys. Chem. A **115**, 1821 (2011).
46. J. Tomlinson-Phillips, J. Davis, D. Ben-Amotz, D. Spangberg, L. Pejov and K. Hermansson, J. Phys. Chem. A **115**, 6177 (2011).
47. G. Hummer, S. Garde, A. E. Garcia, M. E. Paulaitis and L. R. Pratt, J. Phys. Chem. B **102**, 10469 (1998).
48. M. K. Coe, R. Evans and N. B. Wilding, Phys. Rev. Lett. **128**, 045501 (2022).
49. J. H. Griffith and H. A. Scheraga, J. Mol. Struc-Theochem. **682**, 97 (2004).
50. E. Gallicchio, M. M. Kubo and R. M. Levy, J. Phys. Chem. B **104**, 6271 (2000).
51. S. Garde, G. Hummer and M. E. Paulaitis, Faraday. Discuss. **103**, 125 (1996).
52. H. S. Ashbaugh and L. R. Pratt, Rev. Mod. Phys. **78**, 159 (2006).
53. T. Lazaridis, J. Phys. Chem. B **104**, 4964 (2000).
54. D. Paschek, J. Chem. Phys. **120**, 10605 (2004).
55. E. Sobolewski, M. Makowski, C. Czaplewski, A. Liwo, S. Oldziej and H. A. Scheraga, J. Phys. Chem. B **111**, 10765 (2007).
56. P. Setny, R. Baron and J. A. McCammon, J. Chem. Theory Comput. **6**, 2866 (2010).
57. M. Schauperl, M. Podewitz, B. J. Waldner and K. R. Liedl, J. Chem. Theory Comput. **12**, 4600 (2016).
58. A. Das and H. C. Andersen, J. Chem. Phys. **131**, 034102 (2009).
59. L. Lu, S. Izvekov, A. Das, H. C. Andersen and G. A. Voth, J. Chem. Theory Comput. **6**, 954 (2010).
60. J. Jin, Y. Han, A. J. Pak and G. A. Voth, J. Chem. Phys. **154**, 044104 (2021).
61. M. E. Tuckerman, *Statistical mechanics : theory and molecular simulation*. (Oxford University Press, New York, 2010).
62. D. Chandler and D. Wu, *Introduction to modern statistical mechanics*. (Oxford University Press, New York, 1987).
63. G. R. Medders, V. Babin and F. Paesani, J. Chem. Theory Comput. **9**, 1103 (2013).
64. G. A. Cisneros, K. T. Wikfeldt, L. Ojamae, J. B. Lu, Y. Xu, H. Torabifard, A. P. Bartok, G. Csanyi, V. Molinero and F. Paesani, Chem. Rev. **116**, 7501 (2016).
65. A. Das and H. C. Andersen, J. Chem. Phys. **136**, 194114 (2012).
66. V. Molinero and E. B. Moore, J. Phys. Chem. B **113**, 4008 (2008).
67. J. Jin, A. J. Pak, Y. Han and G. A. Voth, J. Chem. Phys. **154**, 044105 (2021).
68. W. G. Noid, J. W. Chu, G. S. Ayton and G. A. Voth, J. Phys. Chem. B **111**, 4116 (2007).
69. J. F. Dama, A. V. Sinitskiy, M. McCullagh, J. Weare, B. Roux, A. R. Dinner and G. A. Voth, J. Chem. Theory Comput. **9**, 2466 (2013).
70. J. Jin, Y. N. Han and G. A. Voth, J. Chem. Theory Comput. **14**, 6159 (2018).
71. J. Jin and G. A. Voth, J. Chem. Theory Comput. **14**, 2180 (2018).
72. J. Jin, Y. N. Han and G. A. Voth, J. Chem. Phys. **150**, 154103 (2019).
73. A. J. Pak, T. Dannenhoffer-Lafage, J. J. Madsen and G. A. Voth, J. Chem. Theory Comput. **15**, 2087 (2019).
74. A. J. Rzepiela, M. Louhivuori, C. Peter and S. J. Marrink, Phys. Chem. Chem. Phys. **13**, 10437 (2011).
75. L. Lu, J. F. Dama and G. A. Voth, J. Chem. Phys. **139**, 121906 (2013).
76. L. Lu and G. A. Voth, J. Chem. Phys. **134**, 224107 (2011).

77.   J. W. Wagner, J. F. Dama, A. E. Durumeric and G. A. Voth, J. Chem. Phys. **145**, 044108 (2016).

78.   B. Song and V. Molinero, J. Chem. Phys. **139**, 054511 (2013).

79.   Y. J. Wu, H. L. Tepper and G. A. Voth, J. Chem. Phys. **124**, 024503 (2006).

80.   W. L. Jorgensen, D. S. Maxwell and J. TiradoRives, J. Am. Chem. Soc. **118**, 11225 (1996).

81.   M. P. Allen and D. J. Tildesley, *Computer Simulation of Liquids*. (Oxford University Press, New York, 1987).

82.   R. W. Hockney and J. W. Eastwood, *Computer simulation using particles*, Repr. ed. (Institute of Physics Publishing, Bristol, 1989).

83.   M. Deserno and C. Holm, J. Chem. Phys. **109**, 7694 (1998).

84.   L. Martinez, R. Andrade, E. G. Birgin and J. M. Martinez, J. Comput. Chem. **30**, 2157 (2009).

85.   M. D. Hanwell, D. E. Curtis, D. C. Lonie, T. Vandermeersch, E. Zurek and G. R. Hutchison, J. Cheminformatics **4** (2012).

86.   W. Humphrey, A. Dalke and K. Schulten, J. Mol. Graph. Model. **14**, 33 (1996).

87.   A. P. Thompson, H. M. Aktulga, R. Berger, D. S. Bolintineanu, W. M. Brown, P. S. Crozier, P. J. I. Veld, A. Kohlmeyer, S. G. Moore, T. D. Nguyen, R. Shan, M. J. Stevens, J. Tranchida, C. Trott and S. J. Plimpton, Comput. Phys. Commun. **271**, 108171 (2022).

88.   Y. Peng, A. J. Pak, A. E. P. Durumeric, P. G. Sahrmann, S. Mani, J. Jin, T. D. Loose, J. R. Beiter and G. A. Voth, (In press).

89.   G. M. Torrie and J. P. Valleau, J. Comput. Phys. **23**, 187 (1977).

90.   S. Kumar, D. Bouzida, R. H. Swendsen, P. A. Kollman and J. M. Rosenberg, J. Comput. Chem. **13**, 1011 (1992).

91.   B. Roux, Comput. Phys. Commun. **91**, 275 (1995).

92.   A. Grossfield, (2012).

93.   M. Bonomi, D. Branduardi, G. Bussi, C. Camilloni, D. Provasi, P. Raiteri, D. Donadio, F. Marinelli, F. Pietrucci, R. A. Broglia and M. Parrinello, Comput. Phys. Commun. **180**, 1961 (2009).

94.   M. Bonomi, G. Bussi, C. Camilloni, G. A. Tribello, P. Banas, A. Barducci, M. Bernetti, P. G. Bolhuis, S. Bottaro, D. Branduardi, R. Capelli, P. Carloni, M. Ceriotti, A. Cesari, H. C. Chen, W. Chen, F. Colizzi, S. De, M. De La Pierre, D. Donadio, V. Drobot, B. Ensing, A. L. Ferguson, M. Filizola, J. S. Fraser, H. H. Fu, P. Gasparotto, F. L. Gervasio, F. Giberti, A. Gil-Ley, T. Giorgino, G. T. Heller, G. M. Hocky, M. Iannuzzi, M. Invernizzi, K. E. Jelfs, A. Jussupow, E. Kirilin, A. Laio, V. Limongelli, K. Lindorff-Larsen, T. Lohr, F. Marinelli, L. Martin-Samos, M. Masetti, R. Meyer, A. Michaelides, C. Molteni, T. Morishita, M. Nava, C. Paissoni, E. Papaleo, M. Parrinello, J. Pfaendtner, P. Piaggi, G. Piccini, A. Pietropaolo, F. Pietrucci, S. Pipolo, D. Provasi, D. Quigley, P. Raiteri, S. Raniolo, J. Rydzewski, M. Salvalaglio, G. C. Sosso, V. Spiwok, J. Sponer, D. W. H. Swenson, P. Tiwary, O. Valsson, M. Vendruscolo, G. A. Voth and A. White, Nat. Methods **16**, 670 (2019).

95.   M. Lauricella, S. Meloni and G. Ciccotti, J. Chem. Phys. **158**, 164501 (2023).